ELSEVIER

Chemical Engineering Science 59 (2004) 4369–4376

Chemical Engineering Science

www.elsevier.com/locate/ces

Mixing in bubble columns: a new approach for characterizing dispersion coefficients

F. Camacho Rubio[a], A. Sánchez Mirón[b], M.C. Cerón García[b], F. García Camacho[b], E. Molina Grima[b], Y. Chisti[c,*]

[a] *Department of Chemical Engineering, University of Granada, E-18071 Granada, Spain*
[b] *Department of Chemical Engineering, University of Almería, E-04071 Almería, Spain*
[c] *Institute of Technology and Engineering, Massey University, Private Bag 11222, Palmerston North 5331, New Zealand*

Received 2 December 2003; received in revised form 15 June 2004; accepted 23 June 2004

Abstract

Use of bubble columns as photobioreactors requires a quantitative knowledge of radial mixing in these columns. A complete model of liquid-phase dispersion was used to simultaneously characterize axial and radial mixing in a relatively large (0.06 m^3, 2.3 m tall, 0.193 m in diameter) bubble column photobioreactor. Axial and radial dispersion coefficients and mixing times were determined in tap water and sea water for superficial aeration velocities of up to 0.051 m s^{-1}. The measured axial dispersion coefficients (D_z) were generally consistent with the predictions of the well established correlations, thus validating the complete dispersion model used in the analysis. The D_z values ranged from $\sim$ 150 to 380 $cm^2\,s^{-1}$ and were highly reproducible. There was evidence that the existing literature data on D_z in bubble columns are slightly underestimated, as consistent underestimation was found to be a characteristic of the widely used dispersion model that disregards radial dispersion. The value of the radial dispersion coefficient was typically about 1% of the D_z value under any given condition. Except at incipient aeration, the radial dispersion coefficient was not as sensitive to the magnitude of the aeration rate as was the axial dispersion coefficient. The mixing time data were generally consistent with the existing correlations.

Keywords: Axial dispersion coefficient; Radial dispersion coefficient; Mixing; Bubble column photobioreactors

1. Introduction

Axial and radial mixing of the liquid phase in bubble columns is characterized by using dispersion coefficients that are analogous to the diffusion coefficient of Fick's law of diffusion. Unlike diffusion, dispersion arises from convective motion of fluid caused by the following main factors: relative movement of the gas and liquid phases; bubble coalescence and break up; the carry forward of fluid in wakes behind the rising gas bubbles and the consequent return flow generated for maintaining mass balance; and turbulence generated by any superimposed flow of liquid. In the past, radial dispersion in bubble columns has generally been lumped with the axial dispersion coefficient and the latter has been used widely and almost exclusively as an index of mixing in such reactors. While substantial information exists on axial dispersion of fluid in bubble columns (Ohki and Inoue, 1970; Towell and Ackerman, 1972; Deckwer et al., 1974; Blenke, 1979; Field and Davidson, 1980; Shah et al., 1982), radial mixing in these reactors has been ignored almost completely. The few measurements of radial dispersion coefficients cited by Deckwer (1992), suggest that the radial dispersion coefficient is always less than one-tenth of the value of the axial coefficient.

When bubble columns are used as photobioreactors, the need arises for quantifying the radial mixing. This is because photosynthesizing microalgae and cyanobacteria suspended in column photobioreactors cause a radial decline in irradiance from a high value near the externally illuminated

* Corresponding author. Tel.: +64-6-350-5934; fax: +64-6-350-5604
E-mail address: y.chisti@massey.ac.nz (Y. Chisti).

0009-2509/$ - see front matter © 2004 Elsevier Ltd. All rights reserved.
doi:10.1016/j.ces.2004.06.037

transparent wall to a low value in the center of the photobioreactor. Consequently, the volume of the photobioreactor can be demarcated into a dark interior core region and a relatively better illuminated peripheral region (Molina Grima et al., 1999, 2000; Sánchez Mirón et al., 1999). The frequency of radial motion of the cell-suspending fluid between the light and dark zones, or the "flashing-light effect", influences the productivity of photobioreactors (Kok, 1953; Terry, 1986; Camacho Rubio et al., 2003). Therefore, ways should be found for quantifying the extent of radial mixing and its dependence on the aeration rate, the main operational variable in a bubble column photobioreactor.

This work presents a theoretical analysis that simultaneously takes into account the axial and radial mixing in bubble columns. This analysis is then used to calculate the axial and radial dispersion coefficients from experimentally measured tracer-response data obtained at various superficial aeration velocities. The relevant experimental techniques for measuring the liquid-phase dispersion have been discussed comprehensively by Deckwer (1992). Dispersion coefficients are generally calculated using the measured concentration-time response to input of a nonreactive, nonabsorptive inert tracer in the reactor. A dispersion model is then used to fit the measured response data. The dispersion coefficient is the model parameter value that best fits the model to the data. This methodology is well established for calculating the axial dispersion coefficient only, as the one-dimensional dispersion model that is typically used for the fitting contains axial dispersion coefficient as the only fitting parameter.

2. Theory

The time course of a tracer's concentration at some measurement location in a bubble column can be described by the following complete dispersion model:

$$\frac{\partial C}{\partial t} = D_z \frac{\partial^2 C}{\partial z^2} - \frac{U_L}{\varepsilon_L}\frac{\partial C}{\partial z} + \frac{D_r}{r}\frac{\partial C}{\partial r} + D_r \frac{\partial^2 C}{\partial r^2}, \tag{1}$$

where C is the tracer concentration at time t, D_z is the axial dispersion coefficient, z is the axial distance from the point of tracer input, D_r is the radial dispersion coefficient, r is the radial distance measured from the center of the column, U_L is the superficial velocity of the liquid in the column, and ε_L is the liquid holdup. Eq. (1) assumes an instantaneous input of the tracer pulse. The liquid holdup in Eq. (1) converts the superficial velocity to the true linear liquid velocity.

Eq. (1) can be made dimensionless using the following definitions of the variables:

$$\theta = \frac{D_z t}{L^2}, \tag{2}$$

$$y = \frac{z}{L}, \tag{3}$$

$$x = \frac{r}{L}\sqrt{\frac{D_z}{D_r}}. \tag{4}$$

In Eqs. (2)–(4), y is the dimensionless axial distance and L is the height of gas–liquid dispersion in the reactor. The dimensionless form of Eq. (1) is

$$\frac{\partial C_T}{\partial \theta} = \frac{\partial^2 C_T}{\partial y^2} - \frac{U_L L}{\varepsilon_L D_z}\frac{\partial C_T}{\partial y} + \frac{1}{x}\frac{\partial C_T}{\partial x} + \frac{\partial^2 C_T}{\partial x^2}, \tag{5}$$

where C_T is the dimensionless tracer concentration defined as follows

$$C_T = \frac{C - C_0}{C_\infty - C_0}. \tag{6}$$

In Eq. (6), C, C_0 and C_∞ are the instantaneous, the initial and the final equilibrium concentrations of the tracer in the liquid batch.

For a batch of liquid in a bubble column, there is no superimposed liquid flow and, hence, $U_L = 0$. Furthermore, considering the cylindrical symmetry of the tracer response and the fact that the wall, the upper surface and the bottom of the reactor are impermeable to the tracer, we have the following:

(i) when $x = 0$, $\partial C_T/\partial x = 0$,
(ii) when $x = R/L\sqrt{D_z/D_r} = \beta$ (i.e. at the wall when $r = R$), $\partial C_T/\partial x = 0$,
(iii) when $\theta > 0$ and $y = 0$, $\partial C_T/\partial y = 0$ (i.e. at the surface of the dispersion),
(iv) when $\theta > 0$ and $y = 1$, $\partial C_T/\partial y = 0$ (i.e. at the bottom of the reactor)

Using the above noted initial and boundary conditions, Eq. (5) can be solved to obtain the following expression for the dimensionless tracer concentration:

$$C_T = \sum_{n=1}^{\infty} \frac{J_0(\upsilon_n x)}{J_0^2(\upsilon_n \beta)} \mathrm{e}^{(-\upsilon_n^2 \theta)} \times \left(1 + 2\sum_{m=1}^{\infty} \cos(m\pi y)\, \mathrm{e}^{(-m^2\pi^2\theta)}\right), \tag{7}$$

where J_0 is the zero-order Bessel function and υ_n is the nth root of the first-order Bessel function, J_1. A similar two-dimensional dispersion model has been used to characterize mixing in liquid–solid fluidized beds (Wei et al., 1995; Chen et al., 2001).

Note that when the C_T in Eq. (7) is radially invariant (i.e. $D_r = \infty$), υ_n, β and x become zero and $J_0 t(\upsilon_n \beta) = J_0(\upsilon_n x) = 1$. In this case Eq. (7) reduces to

$$C_T = 1 + 2\sum_{m=1}^{m=\infty} \cos(m\pi y)\, \mathrm{e}^{(-m^2\pi^2\theta)} \tag{8}$$

which is identical to the solution of the axial dispersion model that was reported by Ohki and Inoue (1970) without considering the radial component of the dispersion.

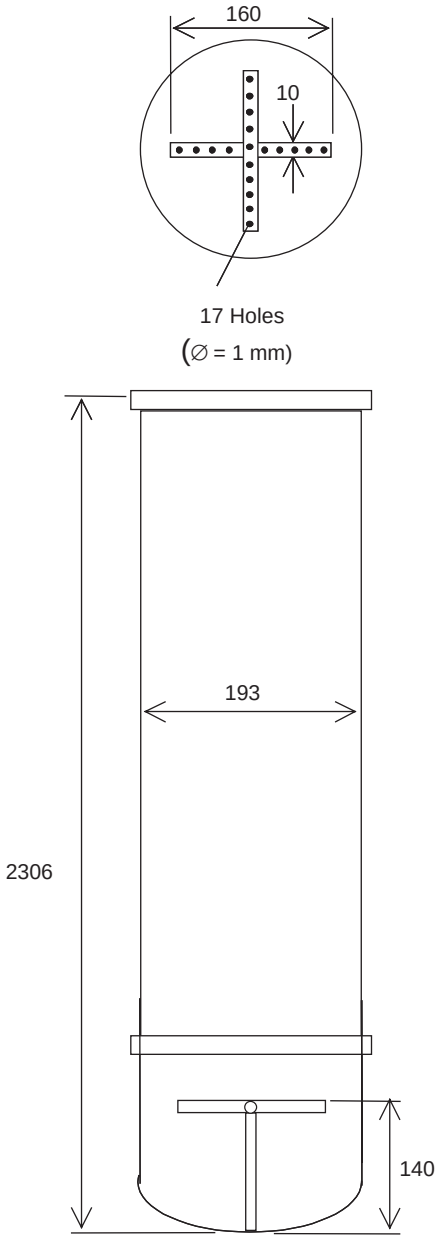

Fig. 1. The geometry of the bubble column and the air sparger. All dimensions in mm.

3. Materials and methods

The bubble column photobioreactor used was made of 3.3 mm thick transparent polymethyl methacrylate, except for a lower 0.25 m section that was made of stainless steel. The vessel had an internal diameter of 0.193 m. The dispersion height was constant at 2.05 m and this provided an approximate working volume of 0.06 m^3. The fluid was mixed by sparging with air through a perforated pipe sparger (17 holes of 1 mm diameter). The superficial aeration velocity varied from 0.00062 to about 0.051 m s^{-1}. The complete geometric details of the vessel appear in Fig. 1.

Measurements were made in tap water and the Mediterranean sea water. Studies in tap water allowed a validation of some of the data by comparing with established correlations. Sea water was used because it is the medium for culturing many microalgae (Sánchez Mirón et al., 1999). The composition of sea water has been published (Contreras et al., 1998). The viscosities of sea- and tap water were 1.278×10^{-3} and 0.998×10^{-3} Pa s, respectively. The viscosities were measured at 20 °C using a Cannon–Fenske viscometer. The surface tension of the fluids were 72.5×10^{-3} and 73.5×10^{-3} N m^{-1} for sea- and tap water, respectively. The surface tension was measured at 20 °C using a platinum–iridium plate tensiometer (KÜSS, model K10DT, Germany).

The acid tracer method (Chisti, 1989) was used to measure the dispersion coefficients as well as the mixing time. Mixing time, which is a direct indicator of the mixing capacity of a reactor, was defined as the time required to attain a 5% deviation from complete homogeneity from the instance of tracer addition. For tracer response measurements, the reactor was filled with the appropriate liquid and the pH was lowered to 2 by adding hydrochloric acid (35% wt/vol). The vessel was then bubbled with air ($U_G \approx 0.03$ m s^{-1}) for 20 min to remove any carbonates in the form of carbon dioxide. The pH was now raised to pH 4.5 by adding 12 M sodium hydroxide. The acid tracer (25 ml of 35% hydrochloric acid) was now added instantaneously at the center of the surface of dispersion. The pH did not go below 2.0. The change in pH with time was measured using 2 pH electrodes. One of these was positioned at specified radial locations (i.e. $r/R = 0$, 0.37 and 0.74) and 0.35 m below the surface of the fluid. The other electrode was positioned at 1.60 m below the surface of the gas-free liquid. The dimensionless concentration C_T of the tracer (hydrogen ion) was calculated as follows:

$$C_T = \frac{[H^+]_{\text{instantaneous}} - [H^+]_{\text{initial}}}{[H^+]_{\text{final}} - [H^+]_{\text{initial}}}. \quad (9)$$

All experiments were carried out in triplicate. The pH data were recorded digitally using an IBM PC compatible computer.

4. Results and discussion

A typical set of the pulse-response data and the best-fit model curve generated using Eq. (7) are shown in Fig. 2. Clearly, the model simulates the measured data closely. The value of the radial dispersion coefficient influenced the height of the model generated peak, whereas the value of the axial dispersion coefficient influenced the width of the peak.

4.1. Axial dispersion coefficient

As shown in Fig. 3, the axial dispersion coefficient increased with increasing aeration velocity irrespective of the

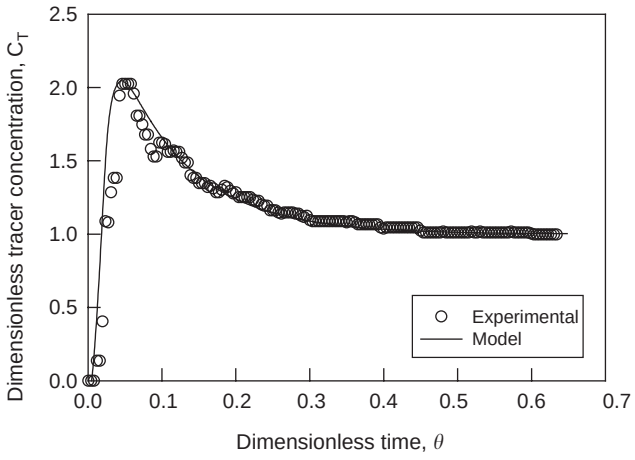

Fig. 2. Measured and the model fitted tracer concentration profiles in the bubble column (sea water, $r/R = 0$; $U_G = 0.051\,\mathrm{m\,s^{-1}}$).

measurement location r/R. For otherwise identical conditions, the values of the axial dispersion coefficient in tap water were generally slightly higher than in sea water. This was because the presence of dissolved salts in sea water reduced the prevailing bubble size compared to the situation in tap water. Small bubbles had small wakes and carried less fluid with them as they rose. In addition, the larger bubbles in tap water underwent more frequent breakup and coalescence and this too increased the axial dispersion coefficient relative to the situation in sea water. As shown by the error bars around selected data points in Fig. 3, the measurements of axial dispersion coefficients were remarkably reproducible in both fluids. The error in replicate measurements was always less than ±10%. The D_z values in Fig. 3 were calculated simultaneously with the radial dispersion coefficient.

The axial dispersion coefficient values measured at the center of the column (i.e. at $r/R = 0$) were generally higher than the values measured at other radial locations (Fig. 3). This was because the local liquid velocity had its maximum value at the center of the column, as evidenced by the numerous measured velocity profiles in the literature (Ueyama and Miyauchi, 1977; Riquarts, 1981; Kawase and Moo-Young, 1989a). Based on these profiles, the bubble columns contain a core zone of liquid upflow (i.e. at $0 \leqslant r/R \leqslant 0.65$). At an approximate r/R value of > 0.7, the liquid flow changes direction. This is the well-known downflow zone adjacent to the bioreactor walls.

The measured values of the axial dispersion coefficients (D_z) were sensitive to "end effects". This is shown in Fig. 4 where the D_z values measured with the pH sensor in the top and bottom locations are compared with the predictions of the following correlations:

$$D_z = 0.343 d^{4/3} (g U_G)^{1/3}, \tag{10}$$

$$D_z = 2.7 d^{1.4} U_G^{0.3}, \tag{11}$$

$$D_z = 0.5 g^{1/4} U_G^{1/2} d^{5/4}. \tag{12}$$

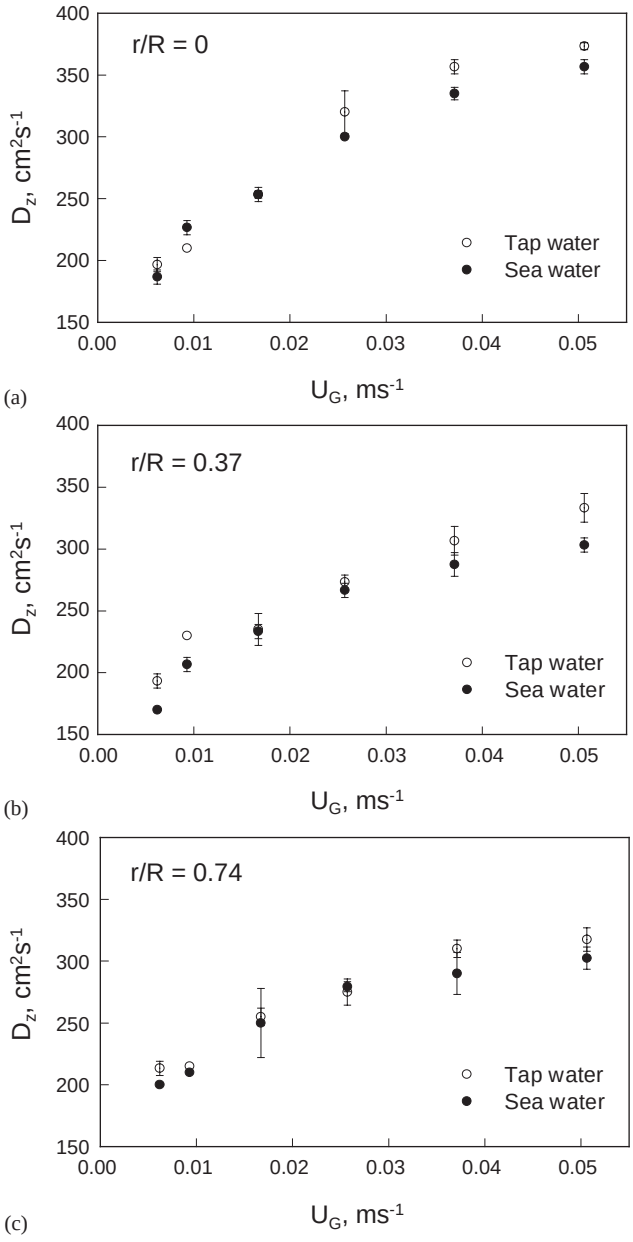

Fig. 3. Effects of the radial measurement position (r/R) and superficial air velocity on axial dispersion coefficient: (a) $r/R = 0$; (b) $r/R = 0.37$; (c) $r/R = 0.74$.

Eqs. (10)–(12) are due to Kawase and Moo-Young (1986), Deckwer et al. (1974), and Miyauchi et al. (1981), respectively. In Eq. (11) the dimensions are in cm. All these correlations were developed for the overall D_z values measured outside the zone of the end effects. As shown in Fig. 4, in both fluids, the D_z values measured close to the top of the column were significantly greater than the values measured at the lower location of the pH sensor. Clearly, the D_z values yielded by the lower pH sensor are in good accord with the available correlations. Unless otherwise specified, the D_z values reported throughout this work were obtained with

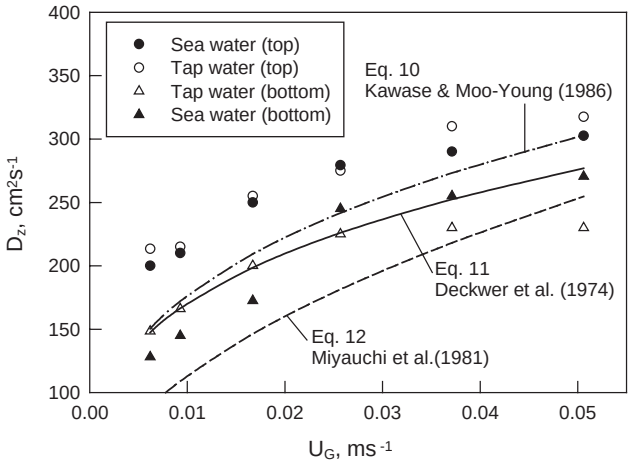

Fig. 4. Comparison of the axial dispersion coefficients measured at the top and bottom located pH probes, with predictions of Eqs. (10)–(12).

the lower pH probe. The radial dispersion coefficient was calculated and noted simultaneously.

Eq. (10) developed empirically, was later shown to have a basis in the mixing length theory (Kawase and Moo-Young, 1989b). Fig. 5 shows the measured D_z data obtained by using models with and without radial dispersion (i.e. Eqs. (7) and (8), respectively), plotted according to the form of Eq. (10). Clearly, the D_z data that does not consider radial dispersion, is quite consistent with the form of Eq. (10). The D_z values computed with the model that took into account radial dispersion (i.e. Eq. (7)) are also consistent with the behavior of Eq. (10), but are consistently slightly higher than the values computed with the model that did not consider radial dispersion (i.e. Eq. (8)). This suggests that all existing data on axial dispersion coefficients in bubble columns is a slight underestimate as all this data were determined without accounting for radial dispersion.

4.2. Radial dispersion coefficient

Fig. 6 shows the radial dispersion coefficient (D_r) values in the fluids, as a function of the aeration velocity. The data shown were obtained at 3 radial locations. Irrespective of the measurement position and the fluid, D_r increased rapidly as the air flow commenced. Further increase in air velocity did not increase the D_r value substantially. The D_r values for sea and tap water were generally similar for otherwise identical conditions. For otherwise equal conditions, the D_r value was typically only about 1% of the D_z value. Mostly, the D_r values measured at $r/R = 0$ were in-between the values measured at $r/R = 0.37$ (i.e. in the upflow core zone of the reactor) and $r/R = 0.74$ (i.e. in the downflow region close to the wall).

The relatively low D_r values were apparently a reflection of the fact that the bubble column operated in the bubble flow regime that exists typically when the superficial

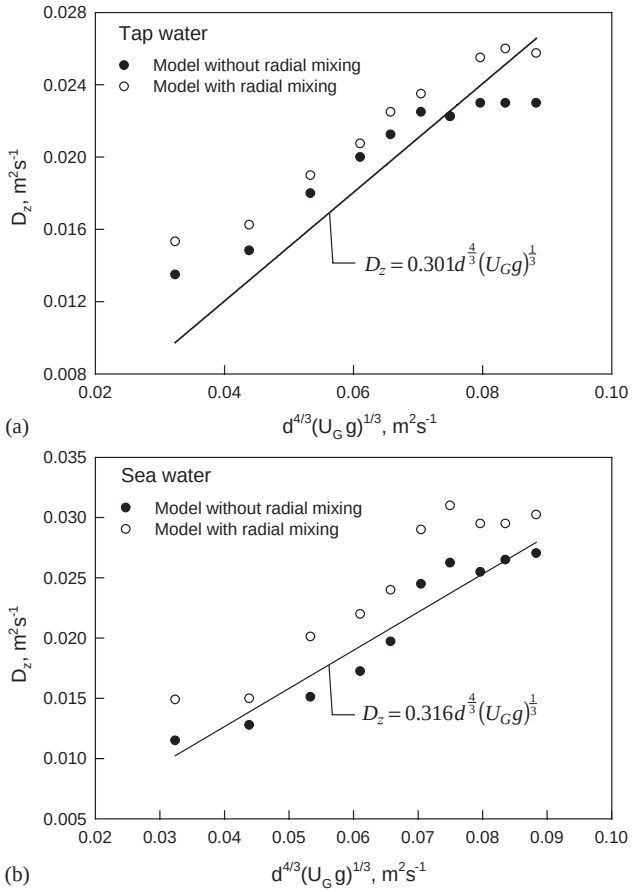

Fig. 5. Comparison of the D_z values estimated using the models with radial dispersion Eq. (7) and without radial dispersion Eq. (8), with equations of the form of Eq. (10): (a) tap water; (b) sea water. The equations shown are the best-fit lines for the filled symbols.

aeration velocity is $\leqslant 0.05\,\mathrm{m\,s^{-1}}$ (Chisti, 1989). Operation in the churn-turbulent flow regime that is characterized by the presence of many spherical cap bubbles, is likely to enhance the D_r value relative to the values shown in Fig. 6. Earlier work in bubble columns have documented the existence of circulating cells of gas and liquid phases in them (Joshi and Sharma, 1979; Deckwer, 1992). The liquid circulation velocity in these cells is made of axial and radial components. Joshi and Sharma (1979) showed that the radial component of the velocity, i.e. the component that is relevant to radial mixing, is only about 36% of the axial component. This explains, at least partly, the relatively poor radial mixing in bubble columns compared to the axial mixing in them.

In contrast to the D_z measurements, the error in the D_r values was much greater (Fig. 6) specially for the measurements at $r/R > 0$. The large deviations from the average in D_r values were probably a reflection of the real random fluctuations in the D_r caused by passage of large bubbles and continual fluctuations of the fuzzy interface between the upflow and the downflow zones.

From the operational point of view of bubble column photobioreactors, it is likely that the D_r values measured at

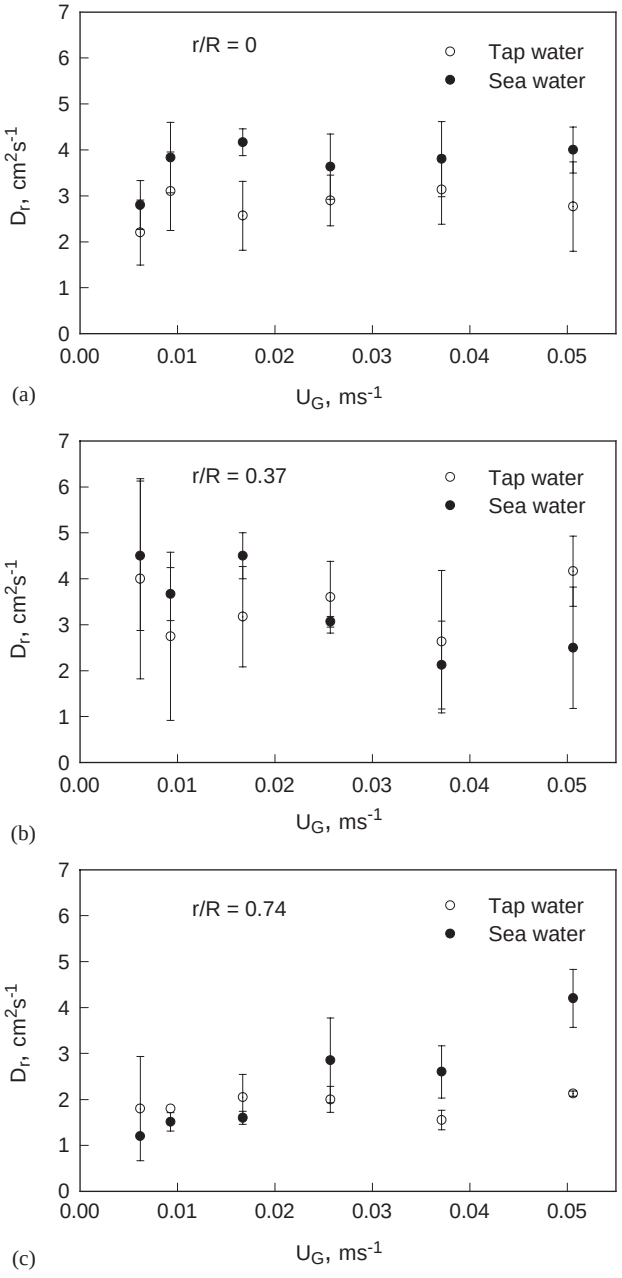

Fig. 6. Effects of the radial measurement position (r/R) and superficial air velocity on radial dispersion coefficient: (a) $r/R = 0$; (b) $r/R = 0.37$; (c) $r/R = 0.74$.

$r/R = 0.74$ are the most relevant ones. This is because the frequency of the interchange of fluid between the relatively well illuminated peripheral zone (i.e. $r/R \geqslant 0.74$) and the darker core (i.e. $r/R < 0.74$) is what affects the productivity of the microalgal biomass. As shown in Fig. 6 ($r/R = 0.74$; sea water), the D_r values increased from nearly one to approximately 4 $cm^2\,s^{-1}$ over the range of air flow rates shown in the figure. In cultures of the microalga *Phaeodactylum tricornutum* in the same bubble column (Sánchez Mirón et al., 2003), increasing aeration rate from 0.01 to 0.05 m s^{-1}

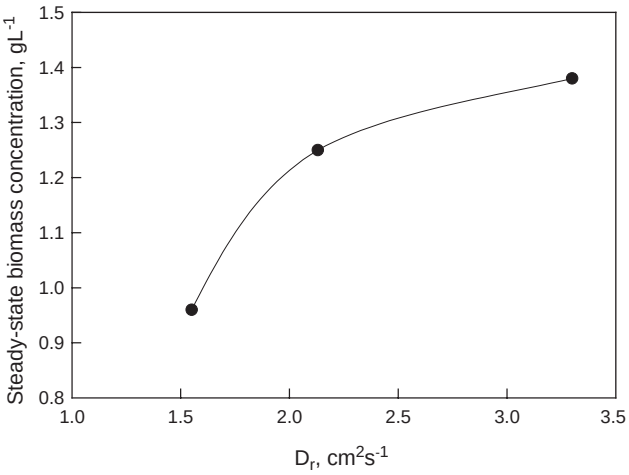

Fig. 7. Steady-state biomass concentration attained at various values of the radial dispersion coefficient. Biomass concentration data were taken from Sánchez Mirón et al. (2003).

was found to increase the steady-state biomass concentration. Plotting the steady-state biomass concentration attained against the D_r values ($r/R = 0.74$) corresponding to the relevant aeration rates (Sánchez Mirón et al., 2003), led to Fig. 7 that demonstrates a strong link between the radial mixing and the attainable biomass productivity of a bubble column photobioreactor. The data in Fig. 7 were obtained at a constant pH of 7.7 controlled by an automatic injection of carbon dioxide. In consequence, the mass transfer of CO_2 was sufficient at all values of D_r.

In the specific geometry of the bubble column used, the bottom depth of 0.25 m consisted of a stainless-steel section that was jacketed for temperature control during culture. The fluid residing in this zone was of course in the dark. Movement of the fluid between this dark zone and the illuminated transparent upper portion of the column was governed mainly by the axial dispersion coefficient D_z. In practice, therefore, a certain light–dark cycling frequency was associated with the axial dispersion of fluid. However, the culture was not likely to have been influenced by this light–dark cycling, for the following reason: even at the lowest aeration rate of 0.01 m s^{-1}, the measured D_z value was 225 $cm^2\,s^{-1}$ (Fig. 3a). Under the same conditions, the D_r value was $\sim 4\,cm^2\,s^{-1}$. Based on these values, an axial liquid velocity was estimated as 225/25, or 9 cm s^{-1}, providing an estimated continuous residence time of $(9/25)^{-1}$ or 2.8 s in the stainless steel dark height. In contrast, using the measured D_r value and the column diameter of 0.193 m, the estimated time for radial movement of the fluid from the center of the column to its periphery was 23.3 s. Clearly, therefore, the presence of the stainless steel bottom zone had a negligible impact on the productivity of the culture compared to the effect of the radial movement of fluid.

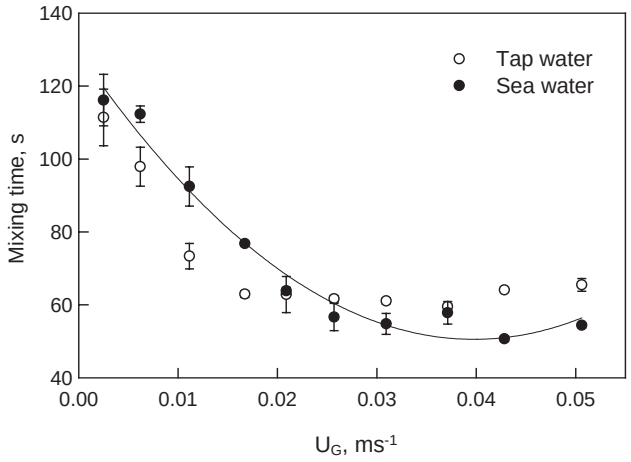

Fig. 8. Mixing time variation with superficial aeration velocity. The solid line is a best-fit trend line for the sea water data.

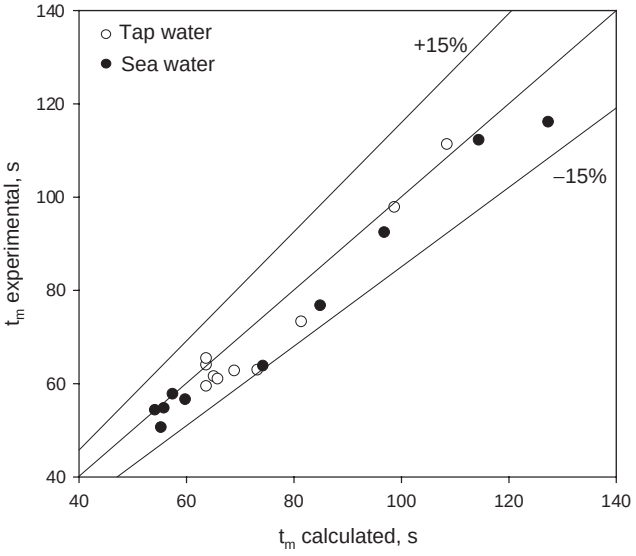

Fig. 9. Measured versus calculated Eq. (13) mixing times in bubble column.

4.3. Mixing time

Mixing time versus aeration velocity data for the bubble column are shown in Fig. 8. For a given aeration rate, the mixing time values in sea and tap water were quite similar (Fig. 8) suggesting that changes in ionic strength above a certain minimal value did not significantly affect the mixing behavior.

Fig. 9 compares the experimental mixing time data with the predictions of the following equation (Kawase and Moo-Young, 1989b) derived from the isotropic turbulence theory

$$t_m = 2^{-\frac{2(1+n)}{3n}} \alpha \frac{L^2}{K d^{4/3} (U_G g)^{1/3}}, \quad (13)$$

where the flow index n is unity for a Newtonian fluid. The α-value for use in Eq. (13) was read from Fig. 3 of Kawase and Moo-Young (1989b) for an injection-detection distance of 1.755 m and a dispersion height of 2.05 m. The α-value was 0.385 and K-value was 0.35. Eq. (13) applied to both tap- and sea water (Fig. 9). The measured data agreed with Eq. (13) within ±15% of exact agreement (Fig. 9); however, Eq. (13) generally tended to overestimate the mixing time values.

5. Concluding remarks

The models traditionally used for describing dispersion in bubble columns take into account only the axial dispersion. This work provides a method for simultaneously quantifying axial and radial dispersion coefficients. The latter are important for establishing the frequency of light–dark cycling of the fluid in bubble column photobioreactors and may be useful for the design of other column-type photoreactors.

The axial dispersion coefficient values determined using the complete dispersion model were generally consistent with the predictions of the existing correlations; however, there was evidence that a disregard of radial dispersion caused a slight but consistent underestimation of the axial dispersion coefficient. The value of the radial dispersion coefficient was typically about 1% of the value of the axial dispersion coefficient under given conditions of operation. The existing correlations were satisfactory for estimating the mixing time in the reactor. As 0.19 m diameter bubble column is the maximum diameter that can be used in photobioreactor applications, the results are directly relevant to full scale photobioreactor engineering purposes. A successful demonstration of the complete dispersion model was achieved for a batch bubble column.

Notation

C	tracer concentration, kmol m^{-3}
C_T	dimensionless tracer concentration defined by Eq. (6)
C_0	initial concentration of the tracer, kmol m^{-3}
C_∞	final or equilibrium concentration of the tracer, kmol m^{-3}
d	diameter of the reactor, m
D_z	axial dispersion coefficient, m^2 s^{-1}
D_r	radial dispersion coefficient, m^2 s^{-1}
e	the number, e
g	gravitational acceleration, m s^{-2}
$[H^+]_{final}$	final tracer concentration, kmol m^{-3}
$[H^+]_{initial}$	initial tracer concentration, kmol m^{-3}
$[H^+]_{instantaneous}$	instantaneous tracer concentration, kmol m^{-3}

J_0	zero-order Bessel function
J_1	first-order Bessel function
K	constant in Eq. (13)
L	height of dispersion, m
n	flow index
r	radial position, m
R	reactor radius, m
t	time or instantaneous time, s
t_m	mixing time, s
U_G	superficial gas velocity based on the diameter of the reactor, m s^{-1}
U_L	superficial liquid velocity based on the diameter of the reactor, m s^{-1}
V_L	linear velocity of the liquid, m s^{-1}
x	dimensionless radial position
y	dimensionless axial position
z	axial distance, m

Greek letters

α	parameter in Eq. (13)
β	parameter in Eq. (7)
ε_L	liquid holdup
υ_n	the nth root of the first-order Bessel function
π	the number pi
θ	dimensionless time

References

Blenke, H., 1979. Loop reactors. Advances in Biochemical Engineering 13, 121–214.

Camacho Rubio, F., García Camacho, F., Fernández Sevilla, J.M., Chisti, Y., Molina Grima, E., 2003. A mechanistic model of photosynthesis in microalgae. Biotechnology and Bioengineering 81, 459–473.

Chen, W., Yang, W., Wang, J., Jin, Y., Tsutsumi, A., 2001. Characterization of axial and radial liquid mixing in a liquid–solid circulating fluidized bed. Industrial & Engineering Chemistry Research 40, 5431–5435.

Chisti, Y., 1989. Airlift Bioreactors. Elsevier, New York, p. 355.

Contreras, A., García, F., Molina, E., Merchuk, J.C., 1998. Interaction between CO_2-mass transfer, light availability and hydrodynamic stress in the growth of *Phaeodactylum tricornutum* in a concentric tube airlift photobioreactor. Biotechnology and Bioengineering 60, 317–325.

Deckwer, W.-D., 1992. Bubble Column Reactors. Wiley, Chichester, pp. 113–156.

Deckwer, W.-D., Burckhart, R., Zoll, G., 1974. Mixing and mass transfer in tall bubble columns. Chemical Engineering Science 29, 2177–2188.

Field, R.W., Davidson, J.F., 1980. Axial dispersion in bubble columns. Transactions of the Institution of Chemical Engineers 58, 228–236.

Joshi, J.B., Sharma, M.M., 1979. A circulation cell model for bubble columns. Transactions of the Institution of Chemical Engineers 57, 244–251.

Kawase, Y., Moo-Young, M., 1986. Liquid phase mixing in bubble columns with Newtonian and non-Newtonian fluids. Chemical Engineering Science 41, 1969–1977.

Kawase, Y., Moo-Young, M., 1989a. Turbulence intensity in bubble columns. Chemical Engineering Journal 40, 55–58.

Kawase, Y., Moo-Young, M., 1989b. Mixing time in bioreactors. Journal of Chemical Technology and Biotechnology 44, 63–75.

Kok, B., 1953. Experiments on photosynthesis by Chlorella in flashing light. In: Burlew, J.S. (Ed.), Algal Culture from Laboratory to Pilot Plant. Carnegie Institution of Washington, Washington, DC, pp. 63–158.

Miyauchi, T., Furusaki, S., Morooka, S., Ikeda, Y., 1981. Transport phenomena and reaction in fluidized catalyst beds. Advances in Chemical Engineering 11, 275–448.

Molina Grima, E., Acién Fernández, F.G., García Camacho, F., Chisti, Y., 1999. Photobioreactors: light regime, mass transfer, and scaleup. Journal of Biotechnology 70, 231–247.

Molina Grima, E., Acién Fernández, F.G., García Camacho, F., Camacho Rubio, F., Chisti, Y., 2000. Scale-up of tubular photobioreactors. Journal of Applied Phycology 12, 355–368.

Ohki, Y., Inoue, H., 1970. Longitudinal mixing of the liquid phase in bubble columns. Chemical Engineering Science 25, 1–16.

Riquarts, H.P., 1981. Flow profiles, change of momentum, and mixing of the liquid-phase in bubble-columns. Chemie Ingenieur-Technik 53, 60–61.

Sánchez Mirón, A., Gómez, A.C., Camacho, F.G., Grima, E.M., Chisti, Y., 1999. Comparative evaluation of compact photobioreactors for large-scale monoculture of microalgae. Journal of Biotechnology 70, 249–270.

Sánchez Mirón, A., Cerón García, M.-C., Contreras Gómez, A., García Camacho, F., Molina Grima, E., Chisti, Y., 2003. Shear stress tolerance and biochemical characterization of *Phaeodactylum tricornutum* in quasi steady-state continuous culture in outdoor photobioreactors. Biochemical Engineering Journal 16, 287–297.

Shah, Y.T., Kelkar, B.G., Godbole, S.P., Deckwer, W.-D., 1982. Design parameters estimations for bubble column reactors. A.I.Ch.E. Journal 28, 353–379.

Terry, K.L., 1986. Photosynthesis in modulated light: quantitative dependence of photosynthesis enhancement on flashing rate. Biotechnology Bioengineering 28, 988–995.

Towell, G.D., Ackerman, G.H., 1972. Axial mixing of liquid and gas in large bubble reactor. Proceedings of the Fifth European Second International Symposium on Chemical Reaction Engineering, vol. B3-1.

Ueyama, K., Miyauchi, T., 1977. Behavior of bubbles and liquid in a bubble column. Kagaku Kogaku Ronbunshu 3, 19–23.

Wei, F., Jin, Y., Yu, Z.Q., Chen, W., 1995. Lateral and axial mixing of the dispersed particles in CFB. Journal of Chemical Engineering Japan 28, 506–510.